Photocatalytic performance of few layer graphitic C_3N_4: enhanced by interlayer coupling

Xianghong Niu[1], Yingwei Yi[3], Jian Zhang [1, 3], Xiaowan Bai[2], Zhaobo Zhou[2], Liang Chu[1], Jianping Yang[1] and Xing'ao Li[1,3*]

[1] New Energy Technology Engineering Laboratory of Jiangsu Province & School of Science, Nanjing University of Posts and Telecommunications (NJUPT), Nanjing 210023, China

[2] School of Physics, Southeast University, Nanjing 211189, China

[3] Key Laboratory for Organic Electronics and Information Displays & Institute of Advanced Materials (IAM), Jiangsu National Synergistic Innovation Center for Advanced Materials (SICAM), Nanjing University of Posts & Telecommunications, Nanjing 210023, China

The evaluation of hydrogen evolution reaction activity

The hydrogen evolution reaction activity of materials can be evaluated by the reaction free energy of hydrogen adsorption (ΔG_H), [1, 2] defined as

$$\Delta G_H = \Delta E_H + \Delta E_{ZEP} - T\Delta S_H$$

ΔE_H is the hydrogen adsorption energy

$$\Delta E_H = E_{(System+H)} - E_{(System)} - \frac{1}{2}E_{H_2} \ .$$

where $E_{(System+H)}$ and $E_{(System)}$ are the energies of g-C_3N_4 systems with and without H adsorption, respectively. ΔE_{ZPE} and ΔS_H are the zero-point energy difference and the entropy difference between the adsorbed and the gas phase, respectively. The ΔE_{ZPE} can be acquired through vibrational frequency calculation. The ΔS_H can be taken as $\Delta S_H = \frac{1}{2}S^0_{H_2}$ because of the fact that the vibrational entropy in the adsorbed state is small on account of previous studies.[1, 3] The optimal value for hydrogen evolution reaction activity is $\Delta G_H = 0$, which means that the smaller values of ΔG_H, the better hydrogen evolution reaction activity performance of materials.

Nonadiabatic molecular dynamics with time-domain density functional theory

We applied *ab initio* nonadiabatic molecular dynamics (NAMD) implemented within time domain density functional theory (DFT) in the Kohn-Sham (KS) framework to model the photogenerated electron dynamics. The Runge-Gross theorem asserts that all observables are determined with the knowledge of the one-body electron density. time domain DFT in the Kohn-Sham approach maps an interacting many-body system onto a system of noninteracting particles where the electron density of the latter equals to the former. The time-dependent charge density of the interacting system can thus be obtained from the time-dependent KS orbitals, $\psi_p(r,t)$ as:

$$\rho(r,t) = \sum_{p=1}^{N_e} |\psi_p(r,t)|^2 \tag{1}$$

The evolution of the electron density is determined by the TD variational principle, leading to a set of single-electron equations for the evolution of the KS orbitals:

$$i\hbar \frac{\partial \psi_p(r,t)}{\partial t} = H(r;R)\psi_p(r,t); p = 1,2,...,N_e \tag{2}$$

By expanding the time-dependent KS orbitals in the adiabatic KS orbital basis, $\phi_p(r;R)$, which is calculated with time-independent DFT from the geometry in the adibatic MD as shown below:

$$\psi_p(r,t) = \sum_k c_k(t)\phi_k(r;R) \tag{3}$$

And by inserting Eq.3 into Eq.2, one can obtain equations for the expanding coefficients:

$$i\hbar \frac{\partial}{\partial t} c_j(t) = \sum_k c_k(t)(\varepsilon_k \delta_{jk} + d_{jk}) \tag{4}$$

Where ε_k is the energy of the adiabatic state *k*, and d_{jk} is the non-adiabatic couplings between the basis *j* and *k*.

The extent of photogenerated electron transfer between active and inactive sites is computed by integrating the projected electron density on active sites (AS).

$$\int_{AS} \rho_{PE}(r,t)dr = \int_{AS} |\psi_{PE}((r),t)|^2 dr = \sum_{i,j} c_i^*(t)c_j(t)\int_{AS} \phi_i^*(r,R(t))\phi_j(r,R(t))dr \tag{5}$$

Taking the time-derivative of eq (5) gives the expression for adiabatic (AD) and non-adiabatic (NA) contributions to charge transfer:

$$\frac{d\int_{AS}\rho_{PE}(r,t)dr}{dt}=\sum_{i,j}\left\{\frac{d(c_i^*c_j)}{dt}\int_{AS}\phi_i^*\phi_j dr+c_i^*c_j\frac{\int_{AS}\phi_i^*\phi_j dr}{dt}\right\} \quad (6)$$

The change in the charge density described by the first term on the right-hand side of eq (6) is due to change of state occupations of the adiabatic KS states, which we refer to as nonadiabatic transfer term. On the other hand, the second term causes change of charge density by change of localization of the KS adiabatic states, hence the name adiabatic transfer. The contribution to the total charge transfer was obtained by further integrating the two terms on the right-hand side of eq (6).

The calculation of binding energy

In order to determine the interaction between g-C_3N_4 layers, the binding energy can be calculated by $E_b=[E_{bilayer}-(2*E_{monolayer})]/n$, where n represents the number of atoms, and $E_{bilayer}$ and $E_{monolayer}$ are the total energies of g-C_3N_4 bilayer vdW heterostructure, the individual g-C_3N_4 monolayers, respectively.

REFERENCES

(1) He, J.; Vasenko, A. S.; Long, R.; Prezhdo, O. V. Halide Composition Controls Electron-Hole Recombination in Cesium-Lead Halide Perovskite Quantum Dots: A Time Domain Ab Initio Study. *J. Phys. Chem. Lett.* **2018,** *9*, 1872-1879.

(2) Greeley, J.; Jaramillo, T. F.; Bonde, J.; Chorkendorff, I. B.; Norskov, J. K. Computational High-Throughput Screening of Electrocatalytic Materials for Hydrogen Evolution. *Nat. Mater.* **2006,** *5*, 909-913.

(3) Lee, Y. M.; Park, J.; Yu, B. D.; Hong, S.; Jung, M. C.; Nakamura, M. Surface Instability of Sn-Based Hybrid Perovskite Thin Film, Ch3nh3sni3: The Origin of Its Material Instability. *J. Phys. Chem. Lett.* **2018**, 2293-2297.

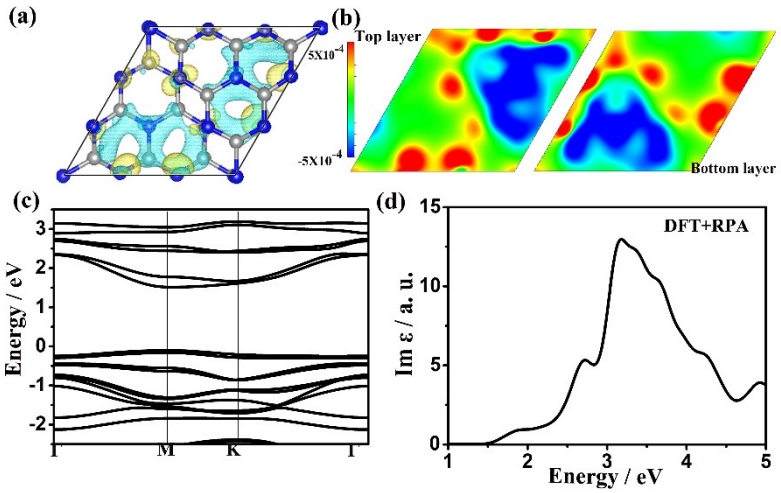

Figure S1. The results are obtained by DFT+PBE+TS method. The difference charge density (a) top view and (b) sectional view of bilayer g-C_3N_4. (c) The bands structure and (d) the imaginary dielectric functions of bilayer g-C_3N_4.

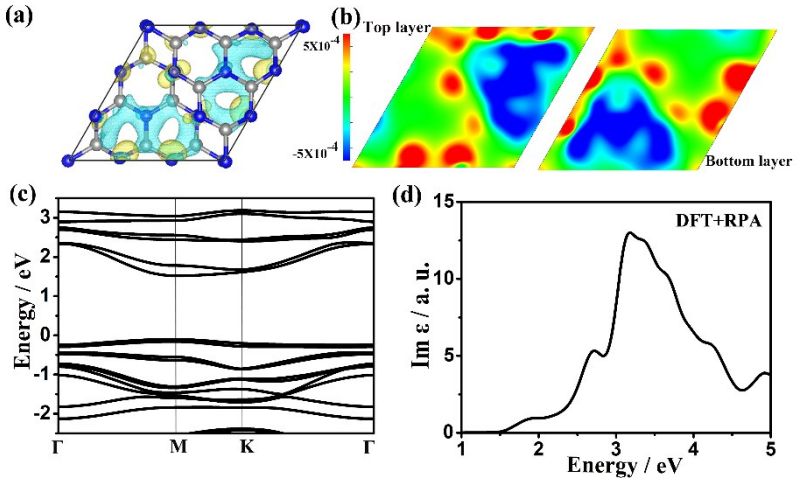

Figure S2. The results are obtained by DFT+PBE+ dDSC method. The difference charge density (a) top view and (b) sectional view of bilayer g-C_3N_4. (c) The bands structure and (d) the imaginary dielectric functions of bilayer g-C_3N_4.

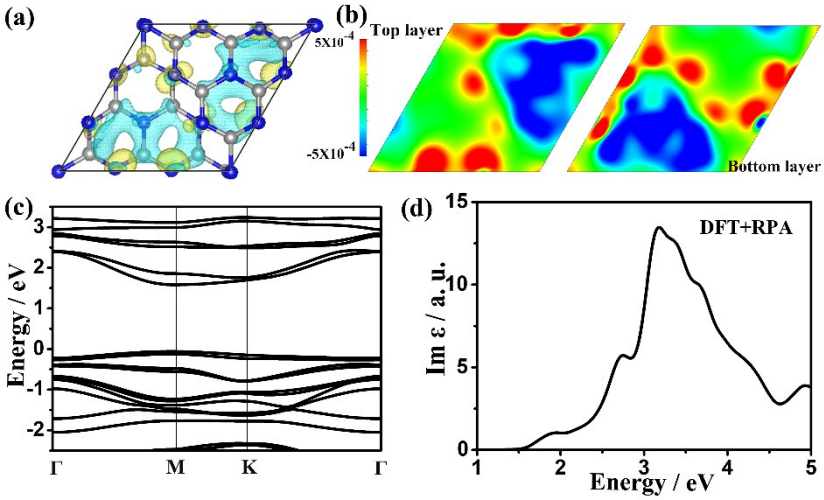

Figure S3. The results are obtained by DFT+PBE+D2 method. The difference charge density (a) top view and (b) sectional view of bilayer g-C_3N_4. (c) The bands structure and (d) the imaginary dielectric functions of bilayer g-C_3N_4.

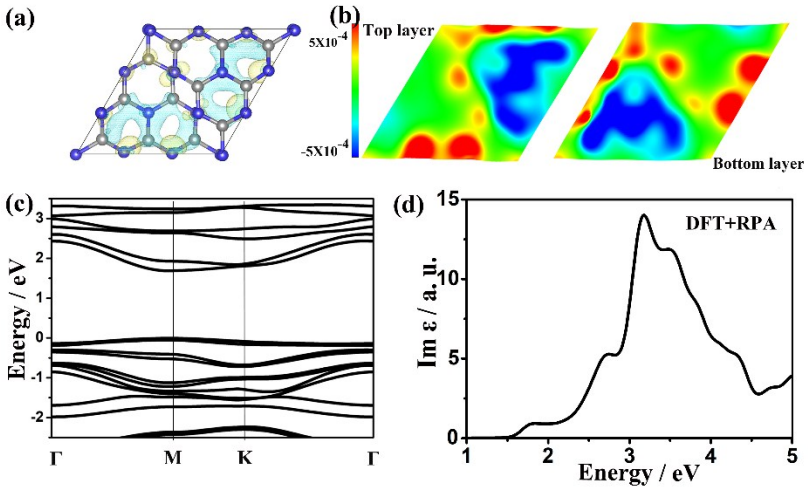

Figure S4. The results are obtained by DFT+PBE+D3 method. The difference charge density (a) top view and (b) sectional view of bilayer g-C_3N_4. (c) The bands structure and (d) the imaginary dielectric functions of bilayer g-C_3N_4.

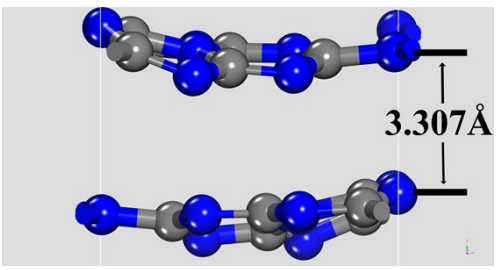

Figure S5. The interlayer distance of g-C_3N_4 bilayer.

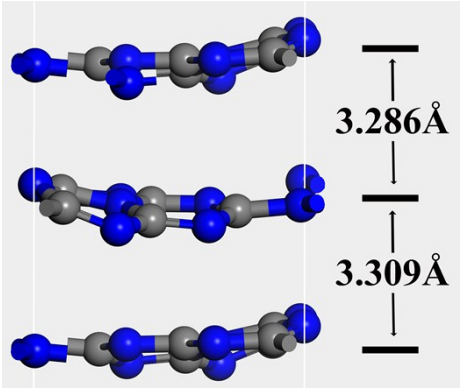

Figure S6. The interlayer distance of g-C_3N_4 trilayer.

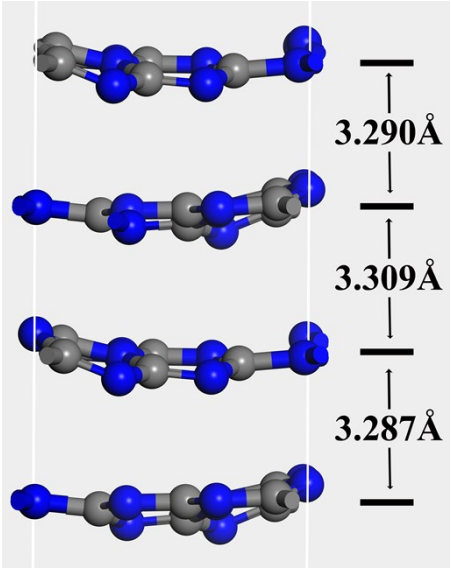

Figure S7. The interlayer distance of g-C_3N_4 four layer.

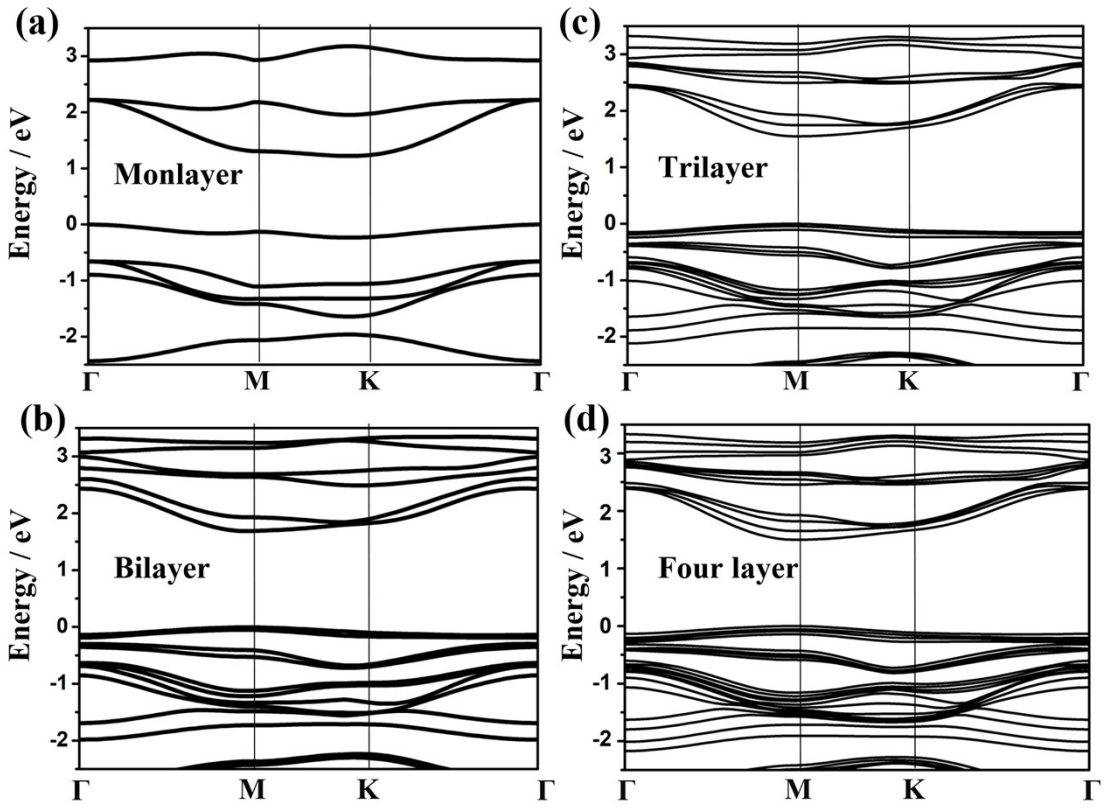

Figure S8. The calculated band dispersion of g-C_3N_4 (a) monolayer, (b) bilayer, (c) trilayer and (d) four layer based on the DFT-PBE level. The VBM of band structure is set as zero. The band gap is 1.22, 1.70, 1.58 and 1.50 eV for g-C_3N_4 monolayer, bilayer, trilayer and four layer, respectively.

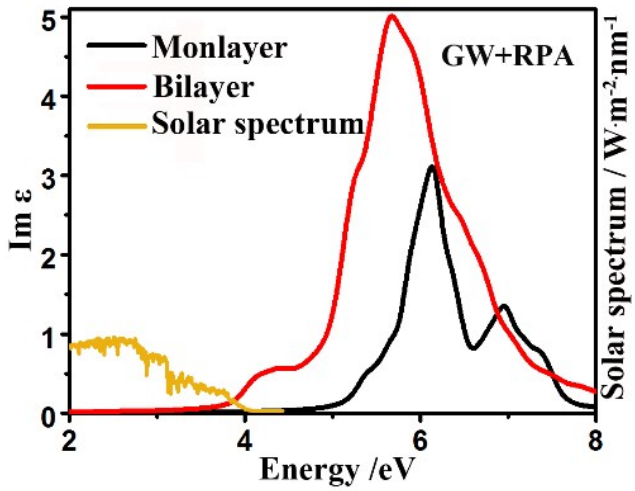

Figure S9. Calculated imaginary dielectric functions of g-C_3N_4 monolayer and bilayer for incident light polarization parallel to the surface based on GW+RPA level, compared with the incident solar flux.